Symmetrical anisotropy enables dynamic diffraction control in photonics

Hicham Mangach, Youssef El Badri, Abdelhamid Hmima, Younes Achaoui, Abdenbi Bouzid, Shuwen Zeng

Research Article | Vol. 31, No. 19 / 11 Sep 2023 / Optics Express 30863
Optics EXPRESS

Symmetrical anisotropy enables dynamic diffraction control in photonics

HICHAM MANGACH,[1,2] YOUSSEF EL BADRI,[2] ABDELHAMID HMIMA,[1] YOUNES ACHAOUI,[2] ABDENBI BOUZID,[2] AND SHUWEN ZENG[1,*]

[1]*Light, Nanomaterials Nanotechnologies (L2n), CNRS-EMR 7004, Université de Technologie de Troyes, 10000 Troyes, France*
[2]*Laboratory of Optics, Information Processing, Mechanics, Energetics and Electronics, Department of Physics, Moulay Ismail University, B.P. 11201, Zitoune, Meknes, Morocco*
[*]*shuwen.zeng@cnrs.fr*

Abstract: Despite the steady advancements in nanofabrication made over the past decade that had prompted a plethora of intriguing applications across various fields, achieving compatibility between miniaturized photonic devices and electronic dimensions remains unachievable due to the inherent diffraction limit of photonic devices. Herein, we present an approach based on anisotropic scaling of the shapes of photonic crystals (PhCs) to overcome the diffraction limit and achieve controlled diffraction limit along the Γ*X* direction. Thus, we demonstrate that scaling the direction perpendicular to the wave's propagation (y-direction) by 1/2 and 1/4 significantly improves the diffraction limit by two and four orders of magnitude, respectively. This approach opens up possibilities for high-frequency wave guiding in a cermet configuration, which was previously unachievable. Furthermore, we illustrate the existence of a quasi-bound state in the continuum (QBICs) in asymmetric dimer network-type photonic crystals (PhCs).

1. Introduction

Mastering the art of wave manipulation has been a centuries-long endeavor, starting with the elderly Greeks to James Clack Maxwell, who sat forth the fundamental framework that underlies our modern understanding of the activity of electromagnetic waves in a medium [1]. Over the last two decades, the advancements made in theory and experiments have enabled the feasibility of endowing artificial materials with wave-handling functionalities beyond the ultimate limitations found in nature, thereby setting a revolutionary milestone in the discipline of optics [2,3]. The emergence of quantum band theory of solids, which stipulates that electronic waves interact with periodically arranged quantum barriers to form a forbidden energy bands, was the earliest spark in the development of these structured materials [4,5]. Photonic crystals (PhCs) were proposed and thoroughly investigated thereafter [6,7]. The notion of one-dimensional stop bands, however, dates back to Lord Rayleigh's demonstration in 1887 that an infinitesimal periodic modulation of the material density within a structure generate a narrow directional band gap, resulting in total reflection [8]. The meteoric rise of this concept was at the forefront of designing a slew of applications wherein the device functionalities are derived from the periodicity of the comprising units. Photonic waveguides, sensors, and graded-index lenses are some of the noteworthy achievements of such synthetic materials [9–11]. Furthermore, miniaturizing dielectric photonic components to attain dimensions comparable to microelectronics has been significantly impacted by diffraction. This makes it extremely difficult to confine light into nanoscale regions smaller than the wavelength, thus significantly decreasing their effectiveness [12,13].

According to the Helmholtz equation, the cavity length of the dielectric slab should be longer than l_0 [14,15], which makes subwavelength confinement of light infeasible in dielectric structures. Moreover, based on the equation $l_0 = \frac{\lambda}{2\sqrt{\varepsilon_r}}$, where ε_r represents the relative permittivity of the

#491396 https://doi.org/10.1364/OE.491396
Journal © 2023 Received 23 Mar 2023; revised 9 Jun 2023; accepted 14 Jul 2023; published 5 Sep 2023

Optics EXPRESS

material, it becomes evident that the length of the cavity is inversely proportional to the refractive index. In this case, if one can use higher refractive index materials, the cavity length can be further reduced. Ebbesen et al.'s pioneering work revealed for the first time in 1998 an extraordinary transmission of light through a perforated metal plate. Their findings showed an unexpected amplification of the transmitted wave beyond the diffraction limit through subwavelength apertures, representing a significant advancement in the field of optics [16]. Recently, negative dielectric permittivity has provided a new paradigm by exploiting subwavelength plasmonic resonance that not only precludes the diffraction barrier but also enhances the electromagnetic energy confinement at the nanoscale [17]. This salient feature has been used to resolve the information carried out through the spatial frequency of evanescent waves, therefore enabling photonic devices to be miniaturized beyond those conventionally available and attain sub-diffraction-limited resolution [18,19]. However, despite all the efforts made by plasmonic materials to bridge the gap between conventional PhCs and nanodevices, this approach still suffers from significant loss dissipation [20]. Nanophotonics based on surface plasmon polaritons (SPPs) offer an appropriate platform for achieving guided SPP modes beyond Abbe's diffraction limit with subwavelength localization of energy, capable of operating both above and below the diffraction limit [13]. By the dawn of the twenty-first century, the emergence of the notion of left-handed metamaterials brought forth tremendous potential in perfect lenses, cloaking invisibility, perfect absorbers, and subwavelength resolution imaging [21–24]. Left-handed metamaterials make single and double negativities accessible through the periodic arrangement of locally resonant meta-atoms [25]. Nonetheless, the inherent complexity of the fabrication process, particularly for 3D nano-architectures, and the fact that this approach is only effective around the resonance frequency, remain some of the major hurdles facing these artificially engineered materials [26].

In this study, we report on a novel approach denoted as the anisotropic scaling effect (ASE) to elevate the diffraction limit in the ΓX direction of dielectric PhCs. We analytically demonstrate the potential modifications imposed by the ASE on the photonic behavior. This is achieved through a modified formalism of the eigenvalue problem, which involves anisotropically scaling Maxwell's equations. Moreover, PhCs are divided into two major categories from a topological standpoint: cermets that are made up of isolated high-density blocks embedded within a low-density host matrix, and networks, which are a density inversion of the previous category in which the patterns are connected to create a more compact structure [27]. In the subsequent sections, we elucidate the potential to elevate the diffraction barrier in these two configurations through the implementation of the ASE. This approach demonstrates an improvement in overcoming the diffraction limit along the ΓX direction in both configurations. A finite element analysis (FEA) is conducted to assess the impact of ASE on the photonic dispersion curves and transmission spectra in both cermet and network configurations. Furthermore, PhCs composed of symmetric and asymmetric dimer of network-type are designed and optimized. The asymmetric dimer PhCs is found to exhibit quasi-bound states in the continuum (QBICs), with a high quality factor of 9.15×10^5 in its transmission response at the point of resonance.

2. Analytical modeling

To establish an analytical description of the scaling effect, we reiterate that anisotropically engineering the unit cells, i.e., introducing a unidirectional scaling factor α onto the geometry, equates to physically scaling the dielectric permittivity distribution along the scaling axis by the same factor. Joannopoulos et al. employed a comparable method to investigate the impact of isotopically scaling the Maxwell's equations, revealing an omnidirectional elevation of the diffraction limit. Nevertheless, when considering the process of nanofabrication, constructing such a highly miniaturized structure using existing technologies poses a significant challenge [28]. Here, we considered scaling the y-direction and leaving the other directions unaltered. Since the dielectric permittivity is scaled by the same factor as the geometry, a proportionate

Optics EXPRESS

anisotropic scaling effect is thus introduced. After performing a variable modification of $r^{'} = r\alpha$, with $r^{'} = \sqrt{x^2 + y'^2 + z^2}$, the resulting dielectric permittivity and differential operator are written as follows:

$$\varepsilon_r^{'}(r^{'}) = \varepsilon_r(r.\alpha) \tag{1}$$

$$\nabla^{'} = \frac{\partial}{\partial x} + \frac{1}{\alpha}\frac{\partial}{\partial y^{'}} + \frac{\partial}{\partial z} \tag{2}$$

By inserting the new differential operator and dielectric function into the Helmholtz equation, a new eigenvalue problem for a nonmagnetic dielectric medium is described [29]:

$$\frac{1}{\varepsilon_r^{'}(r^{'})}\alpha\nabla^{'} \times [\alpha\nabla^{'} \times E(r^{'}, t)] = \frac{\omega^2}{c^2}E(r^{'}, t) \tag{3a}$$

$$\frac{1}{\varepsilon_r^{'}(r^{'})}\nabla^{'} \times [\nabla^{'} \times E(r^{'}, t)] = (\frac{\omega}{\alpha c})^2 E(r^{'}, t) \tag{3b}$$

where $\varepsilon_r^{'}(r^{'})$, ω and c are the relative dielectric permittivity, the angular frequency and speed of light in vacuum, respectively.

The optical wave propagates along the x-axis, which implies that it only experiences the unaltered modulated medium. Furthermore, the equation indicates that the new frequency $\omega^{'} = \frac{\omega}{\alpha}$ is greater since the scaling factor is less than unity. Thus, theoretically confirming that the frequency is scaled by α, resulting in the shifting of the diffraction limit towards higher frequencies. The Floquet-Bloch theorem was then applied along the x and y-axes to investigate the 2D PhC model. According to the latter theorem, the solution of a periodic potential can be expressed as the product of a plane wave and a periodic function with the same periodicity as the crystal [30].

$$\Psi(r^{'}) = E(r^{'})u(r^{'}) \tag{4}$$

where $u(r^{'}) = u(r^{'} + a)$ is a periodic function with the same period as the crystal. Equation (4) presents the mathematical formulation of the Floquet-Bloch theorem, which encounter challenges associated with negative eigenvalues. To overcome this concern, one can employ the Fourier basis and represent the periodic function in the form of a Fourier series, as illustrated by Eq. (5):

$$f(r^{'}) = \sum_G f_G \, exp(iGr^{'}) \tag{5}$$

G symbolizes a set of reciprocal lattice vectors. However, our study specifically focuses on transverse electric waves with an out-of-plane electric field component denoted by E_z. The choice of transverse electric (TE) mode is determined by the symmetry of the unit cell, specifically mirror and rotational symmetries. Transverse magnetic (TM) mode can only be supported when there is rotational symmetry within the unit cell. This distinction arises from the fact that the electric field (E) behaves as a vector, while the magnetic field (H) behaves as a pseudovector. Consequently, the magnetic field maintains its direction during the mirror symmetry operation [28].

3. Network configuration

For the sake of delineating the feasibility of utilizing the anisotropic scaling effect to produce network-type PhCs with an adjustable diffraction limit frequency, we first consider a typical 2D PhC with a spatial period a, and an air-gap rectangular defect with a preset filling factor of f, as indicated in Table. 1. The unit cell is perfectly symmetrical along the x and y-axes, as depicted in Fig. 1(a), the rectangular air-gap in this case has a width of $0.6\,a$ and a height of $0.9\,a$. It will serve as a reference for all subsequent numerical simulations conducted in this section. Concerning the

Optics EXPRESS

network-type PhCs, we opted for silicon material as the high-optical density host matrix and air as low-optical density inclusions to form the network pattern. Furthermore, silicon is produce on a large-scale in the industry, and it is considered one of the most essential materials on the frontiers of modern technology. Owing to its potential in on-chip photonic device manufacturing for light confinement, silicon PhC technology has matured to the point where it outperform the photovoltaic and electrical industries [31,32]. For all the reasons stated above, we have taken a keen interest in building our structures with monocrystalline silicon. All materials used in this work are assumed to be dispersive and loss free. The refractive index of silicon in the relevant region is about $n_{Si} = 3.5$, whereas that of air is assumed to be a constant value of $n_{Air} = 1$.

Photonic band diagrams are constructed through solving the eigenfrequency problem using the FEA to investigate the optical properties of such regularly spaced inclusions, and a harmonic analysis is carried out to assess the transmission spectra. To do so, we build an array of $N_x \times N_y$ unit cells with an electromagnetic wave propagating freely in the two regions on the left and right sides of the array. We applied the TE polarized harmonic excitation source E_z at the left side of the x-axis and a detector on the right side. A periodic condition was also applied in the y-direction to assume that the crystal is infinite along the perpendicular direction of the wave's propagation.

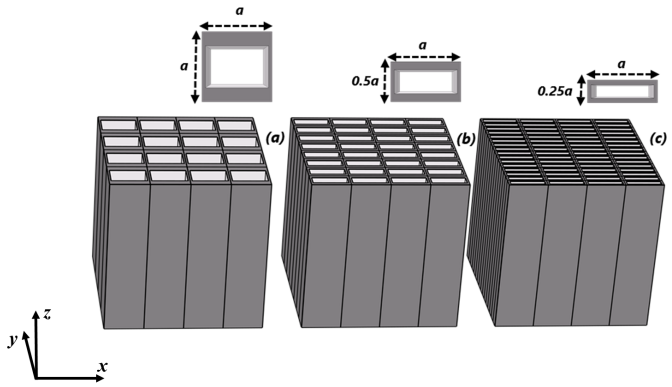

Fig. 1. Illustrations of the PhC structures studied: (a) Conventional silicon PhC with symmetric unit cell. (b) and (c) the halved (0.5 a) and quartered (0.25 a) PhCs, respectively.

Table 1. Structural characteristics of network-type PhCs in normal, halved, quartered, symmetric, and asymmetric dimer configurations

a	f	*scaling*	T_1	T_2	N_x	N_y
$1[\mu m]$	0.54	$1, 1/2, 1/4$	$100[nm]$	$30[nm]$	7	1

The first Brillouin zone is recognized as the smallest region of the reciprocal lattice that includes all reciprocal lattice points. When the reciprocal lattice exhibits significant symmetry, the study of photonic crystals can be narrowed down to the irreducible Brillouin zone. This enables a focused analysis of the photonic crystal's fundamental properties and behavior, emphasizing the essential core or basic building block within the irreducible Brillouin zone. In square lattice (conventional PhCs), the irreducible Brillouin zone exhibits high symmetry points that are denoted as Γ, X, and M, as elucidated in Fig. 2(d). Where, Fig. 2(e) represents the rectangular lattice, which encompasses halved and quartered PhCs and contains high symmetry points designated as Γ, X, S and Y in its first non irreducible Brillouin zone. However, within the scope of this study, we emphasize that even though we analyzed the eigenmodes in the whole irreducible Brillouin zone,

Optics EXPRESS

as shown Fig. 2, we are solely interested in the modes exhibited along the ΓX direction due to the unidirectional nature of the ASE that we proposed.

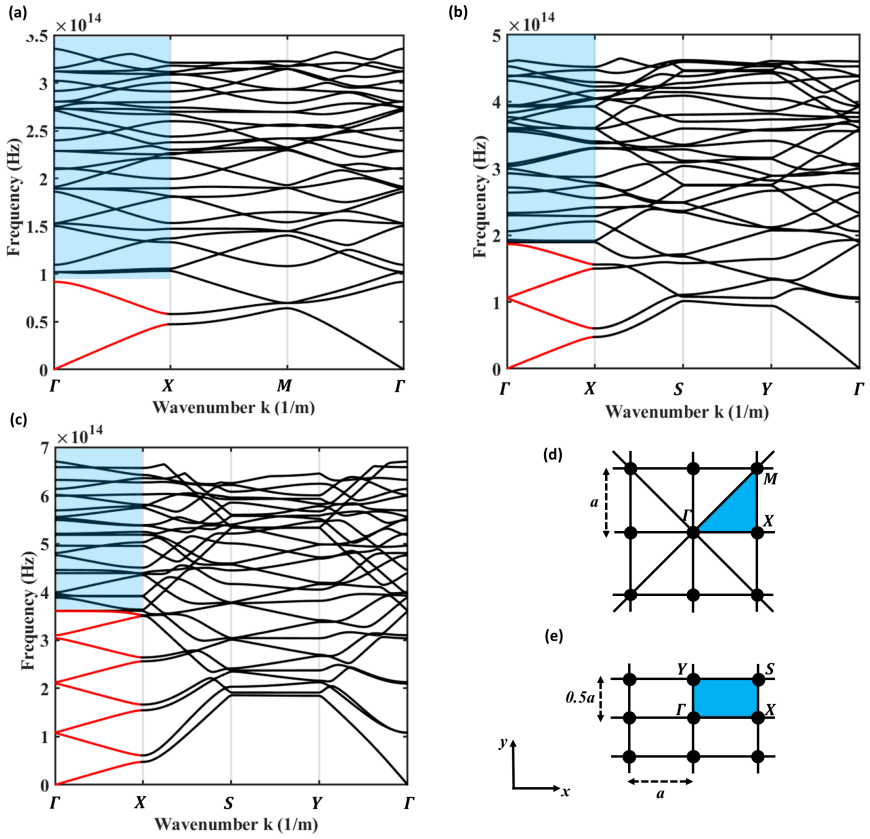

Fig. 2. Transverse electric (TE) photonic band diagrams within the irreducible Brillouin zone for three types of network PhCs: (a) conventional, (b) the halved, and (c) the quartered. The diffraction curtain, presented by a light-blue color, is specifically highlighted along the ΓX direction, with a wavenumber of $k_x \in [0, 1 \times \pi/a]$. The modes highlighted in red depicts the band folding phenomenon of the first mode, wherein the extension occurs as the scaling parameter α changes from 1 to 1/4. (d, e) Illustrations of the Brillouin zone for the conventional PhCs (square lattice) and anisotropically scaled PhCs (rectangular lattice).

Bragg diffraction is a restriction that greatly affects the performance of engineered periodic structures, effectively preventing their operation in the high-frequency range. Figure 2(a) serves as an illustrative example, displaying the appearance of the diffraction curtain after the first band folding in ΓX direction. Consequently, conventional photonic devices can only operate at low frequencies, located below the diffraction barrier. Extending their operation range to much higher frequencies remains a priority, and this attribute is accomplished only through the development of subwavelength structures, which is a result of technological progress. Indeed, several strategies have been developed to sidestep this barrier, harnessing both the available materials in nature and the range of artificially manufactured ones. Surface plasmon-based photonics, which combine photonic characteristics with electronics miniaturization [12], and photonic nanojets with waists smaller than the diffraction limit, which allow light to pass through without significant diffraction [33], have been reported. Figure 2(b) and Fig. 2(c) illustrate the diffraction curtain (blue regions in ΓX direction) being elevated by a factor of two and four in the

Optics EXPRESS

cases of the halved and quartered network-type PhCs, respectively. It is important to highlight that the evaluation of the corresponding transmission spectra for these network-type photonic crystals (PhCs) was exclusively conducted in the Γ*X* direction. This deliberate choice was made due to the specific nature of our approach, which is tailored for this particular direction.

The corresponding transmission spectra of these network-type PhCs are depicted in Fig. 3. These results are in good accordance with the dispersion diagrams in Γ*X* direction, where the blue regions indicate the Bragg limit position for each of the introduced structures. The diffraction limit in network-type PhCs occurs at 0.95×10^{14} Hz for the conventional structure, 1.9×10^{14} Hz for the halved structure, and 3.8×10^{14} Hz for the quartered structure. These diffraction limit values are determined using the Bragg diffraction formula and confirmed via numerical simulation. Thus, our approach based on architectural engineering to overcome the diffraction constraint, although unidirectional, provides a powerful tool for elevating the diffraction limit. Due to the reasons discussed above, the practical application of conventional photonic crystals (PhCs) is typically limited to the first band folding regime, where the wavelength of light is significantly greater than the spatial periodicity ($\lambda >> 2a$). This is because Bragg diffraction occurs when the wavelength of light becomes comparable to the spatial periodicity. In Fig. 4, we present a scenario featuring a 1D layer of PhCs with dimensions of 5, 10, and 20 periods for the conventional, halved, and quartered network-type PhCs, respectively. We specifically highlight the influence of the direction perpendicular to the wave propagation by considering the 1D layer of PhCs as a diffraction grating with a periodicity in the *y*-direction of a, $0.5a$, and $0.25a$. At lower frequencies, particularly at 0.65×10^{14} Hz, all configurations effectively perform with respect to TE polarized wave excitation, as depicted in Fig. 4(a-c). However, at the frequency of 1.5×10^{14} Hz, the conventional 1D layer becomes diffraction limited, whereas the halved and quartered 1D layers remain free from diffraction effects, as seen in Fig. 4(d-f). At a much higher frequency of 2.9×10^{14} Hz, both the conventional and halved 1D layers are subjected to diffraction, while the quartered 1D layer remains diffraction-free, as shown in Fig. 4(g-i).

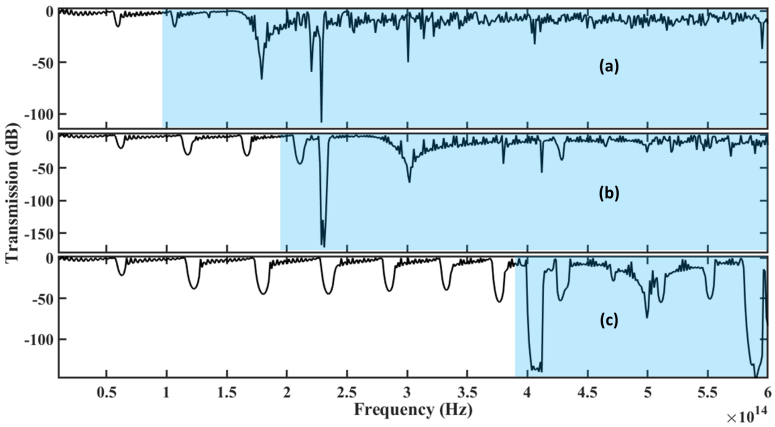

Fig. 3. Transmissions of transverse electric (TE) polarized waves along the Γ*X* direction: (a) network-type conventional PhC (top), (b) halved PhC (middle), and (c) quartered PhC (bottom).

Figure 5(a) illustrates the design of an array of symmetric dimers. Each unit cell has a total width of half a period, obtained by arranging two quartered PhCs in the *y*-direction. We construct an array of asymmetric dimers by appropriately matching the spacing between the two air gaps within the symmetric dimers, as seen in Fig. 5(b). The eigenvalue computations in Γ*X* direction of symmetric and asymmetric dimers of network-type PhCs delineate that the symmetric case retains the primary feature of the quartered network-type PhC scenario, except that the optical

Optics EXPRESS

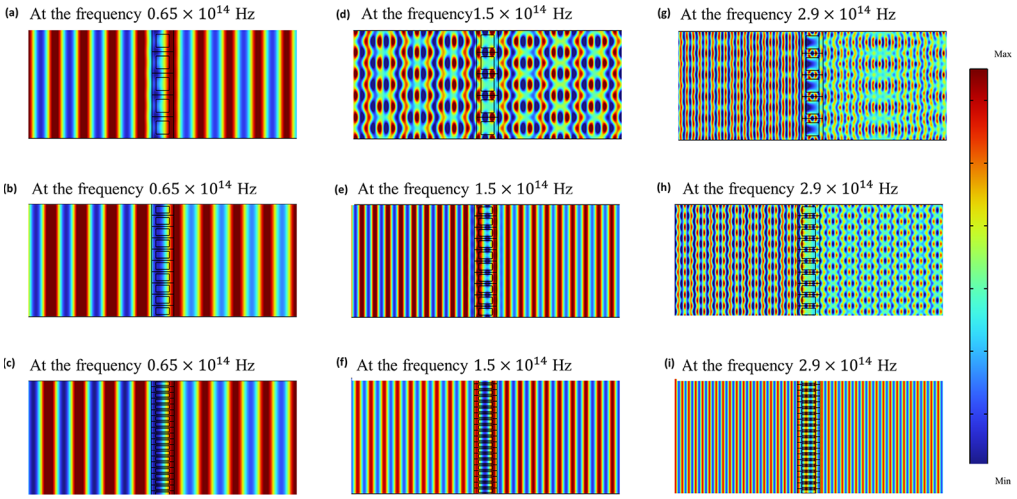

Fig. 4. (a-c) The distribution of the out-of-plane electric field (Ez) after interacting with a single layer of photonic crystals arranged along the *y*-axis, for normal (a), halved (0.5a), and quartered PhCs (0.25a), at a frequency of 0.65×10^{14} Hz. (d-e) The distribution of the electric field Ez at a frequency of 1.5×10^{14} Hz for normal, halved, and quartered PhCs, respectively. (g-i) The distribution of the electric field for normal, halved, and quartered photonic crystals at a frequency of 2.9×10^{14} Hz, respectively.

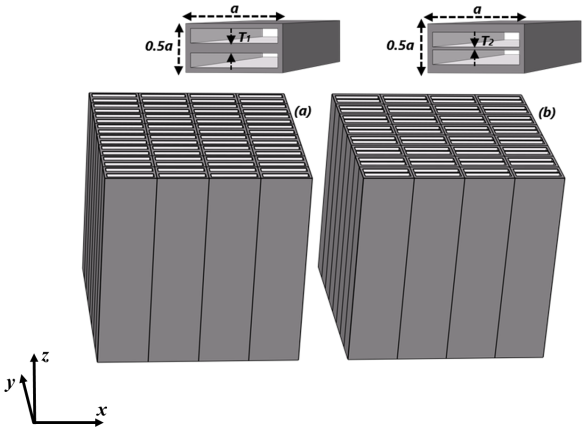

Fig. 5. Representations of the dimer network-type PhCs studied: (a) Symmetric dimer, and (b) Asymmetric dimer.

wave encounters a unit cell with a half period, which results in a band overlap after the third band folding, as indicated in Fig. 6(a). The transmission spectrum remains unaltered, confirming the hypothesis that band overlapping is unrelated to the diffraction phenomenon. The asymmetric dimer case exhibits a sharp transmission response due to the asymmetry of inclusions within it, which corresponds to a steady mode with a near-zero group velocity marked in blue, as can be seen in Fig. 6(b). A more detailed analysis using harmonic study is employed to selectively excite the localized mode and evaluate the corresponding quality factor by varying the asymmetrical factor (S). The asymmetrical factor is defined as follows:

$$S = 1 - \frac{T_2}{T_1} \tag{6}$$

Optics EXPRESS

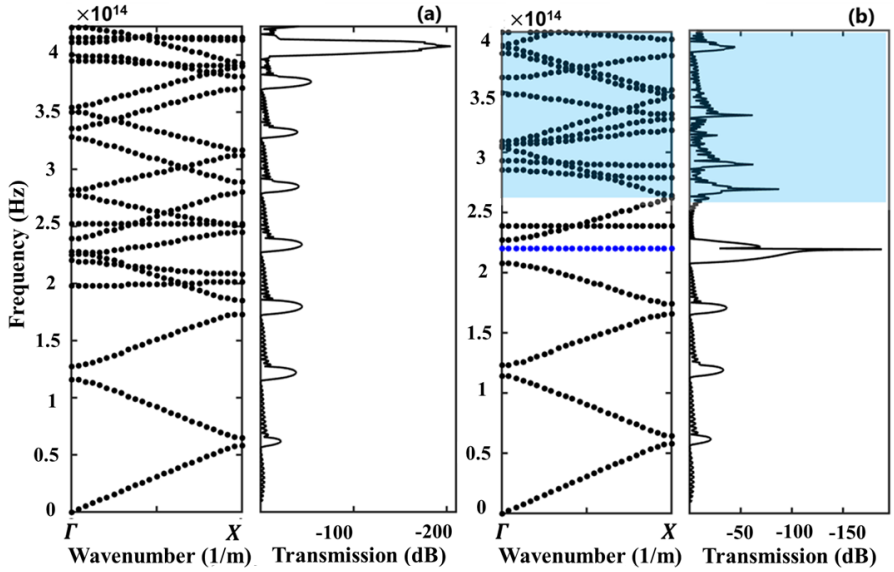

Fig. 6. Dispersion diagrams and corresponding transmission signatures of transverse electric (TE) waves for symmetric (a) and asymmetric (b) dimer network-type photonic crystals (PhCs) along the ΓX direction with a wavenumber of $k_x \in [0, 1 \times \pi/a]$.

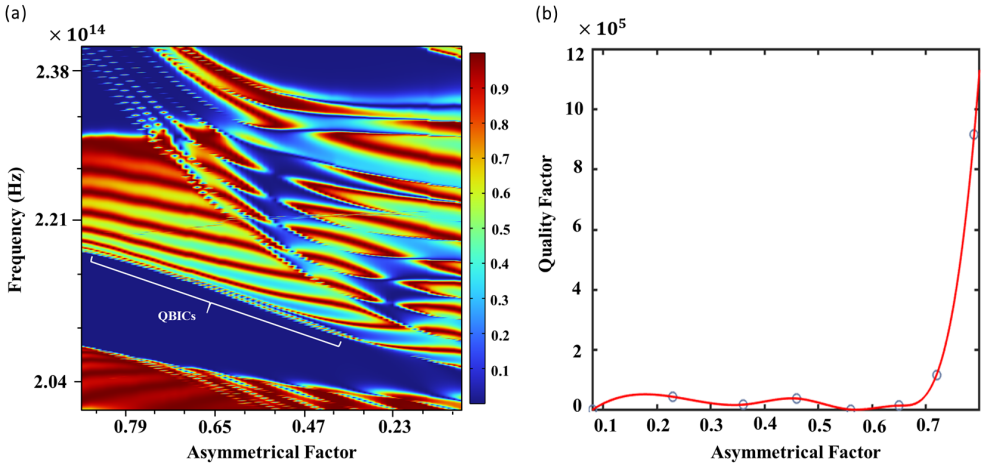

Fig. 7. (a) The shift of the Quasi bound states in the continuum (QBICs) position with different degrees of the asymmetrical factor in asymmetrical dimer network-type PhCs. (b) Analysis of the relationship between the quality factor and the level of asymmetrical factor in asymmetrical dimer network-type PhCs.

Through this analysis, we demonstrate the presence of quasi-bound states in the continuum (QBICs) that emerge with an increasing asymmetrical factor. Figure 7(a) demonstrates the shift of these QBICs as a function of the asymmetrical factor. It is noteworthy that at lower values of (S<0.2), only interference phenomena occur, while at approximately (S>0.2), the existence of specific exotic states becomes apparent at the upper edge of the band gap. The concept of bound states in the continuum (BICs), also referred to as dark states, characterizes a condition in which there is no radiation coupling [34]. In this condition, the energy becomes highly

Optics EXPRESS

concentrated in the near field and possesses an infinite lifetime, unable to be radiated into the far field [35]. Moreover, QBICs exhibit the capability to concentrate and confine electromagnetic waves within subwavelength dimensions [36,37]. Consequently, they enable the demonstration of a supercavity mode with a significantly high quality factor (Q-factor) [38]. Figure 7(b) depicts the evolution of the quality factor (QF) as a function of the asymmetrical factor (S). The QF exhibits fluctuations due to the sensitivity of these QBICs to the asymmetrical factor. Notably, a high QF is achieved when the asymmetrical factor reaches $S = 0.73$, indicating the presence of a pronounced resonance in the system that meets the stringent sensing requirements.

4. Cermet configuration

In contrast to the network-type PhCs previously discussed, cermet-type PhCs have high-density optical inclusions (silicon) in a matrix with low-density optical material (air). Table 2 outlines the new geometrical parameters of the cermet configuration. Figure 8(a) depicts cermet-type PhCs with the same spatial period as network-type PhCs [39]. The width and height of silicon pillars are equal to $0.6\,a$, whereas Fig. 8(b) and Fig. 8(c) illustrate the halved and quartered cermet configurations.

Figure 9 reveals the potential of the ASE to raise the diffraction curtain toward higher frequencies while sustaining large bandgaps within each band folding. The locations of the sharp decreases in transmission perfectly match the bandgaps for each trial, as shown in Fig. 10. Therefore, the transmission spectra are consistent with the dispersion diagrams, indicating that the Bragg limit in cermet-type PhCs jumps from 1.025×10^{14} Hz for the standard, to 2.05×10^{14} Hz for the halved, to 4.01×10^{14} Hz the for the quartered case. The dispersion diagrams of the cermet-type PhCs reveal large band gaps, which have important implications for various applications, such as energy harvesting and electromagnetic wave guiding [40,41]. Previous research on cermet-type PhCs has employed energy localization in the flat mode. Our objective was to investigate the feasibility of using ASE to create cermet-type PhCs capable of effectively steering high-frequency electromagnetic waves, which were previously limited by the diffraction constraint. To this end, we constructed a superlattice consisting of $(N_x' \times N_y')$ unit cells of conventional, halved, and quartered cermet-type PhCs with defects along the y-direction. The defects utilized consist of a straight lines of silicon inclusions. Figure 11(a) and Fig. 11(b)

Table 2. Geometrical parameters of cermet-type PhCs configuration

a	f'	*scaling*	N_x'	N_y'
$1[\mu m]$	0.36	$1, 1/2, 1/4$	8	11

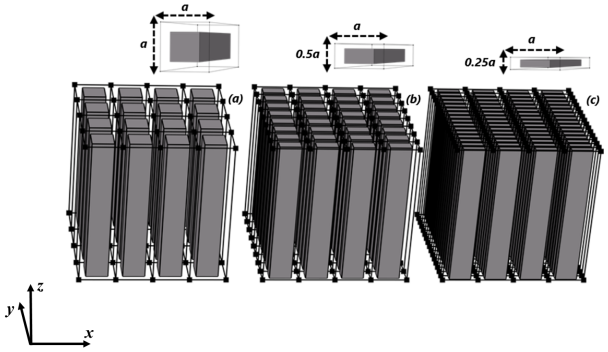

Fig. 8. Cermet-type configurations studied: Panel (a) represents the ordinary PhC, while panels (b) and (c) exhibit the halved and quartered PhCs, respectively.

Optics EXPRESS

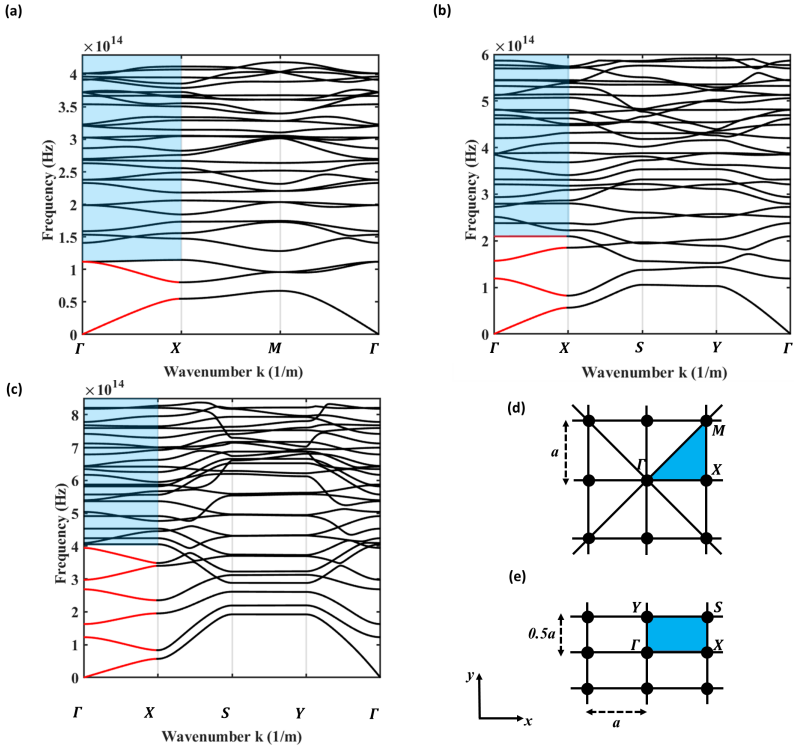

Fig. 9. Transverse electric (TE) photonic dispersion spectra in the irreducible Brillouin zone for the conventional (a), halved (b) and quartered (c) cermet-type configurations. The diffraction curtain is highlighted only along the ΓX direction with a wavenumber of $k_x \in [0, 1 \times \pi/a]$. (d, c) Illustrations of the Brillouin zone for the conventional PhCs (square lattice) and anisotropically scaled the (rectangular lattice)

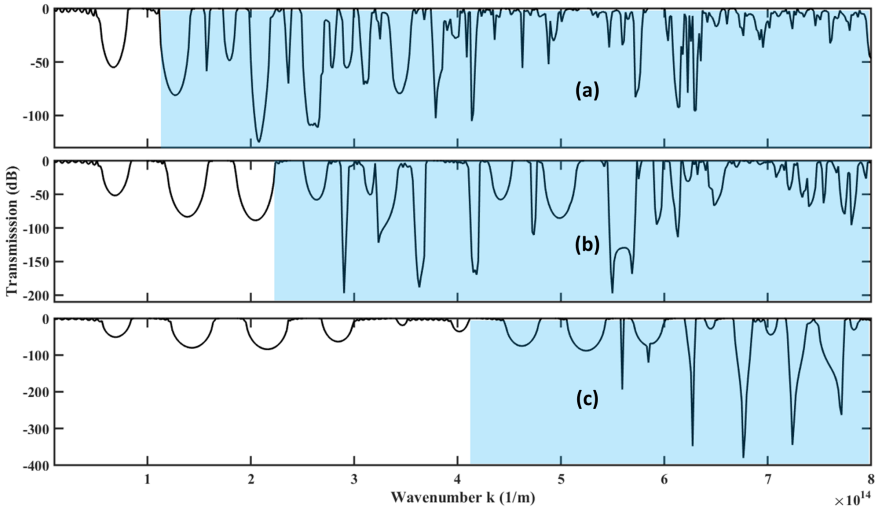

Fig. 10. The transmission signatures of transverse electric polarized waves (TE) in the cermet-type configurations. (a) Depicts the ordinary PhC structure, while (b) and (c) illustrate the halved and quartered PhC structures, respectively along the ΓX direction.

Optics EXPRESS

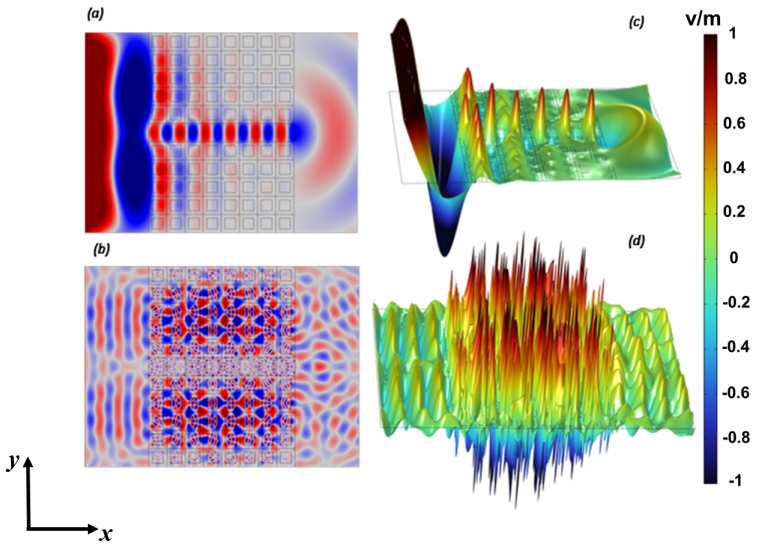

Fig. 11. The distributions of the out-of-plane electric field component and their high expressions are depicted for ordinary cermet-type PhC. Panels (a) and (c) correspond to the first band folding at a frequency of 0.7×10^2 THz, while panels (b) and (d) illustrate the diffraction zone at a frequency of 3×10^2 THz.

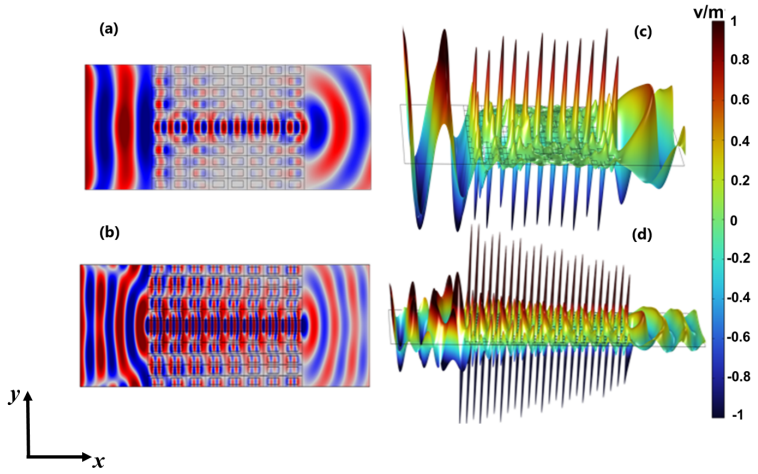

Fig. 12. The distributions and high expressions of the out-of-plane electric field component for halved and quartered cermet-type PhCs. Maps (a) and (c) depict the halved PhC at the second band folding frequency of 1.4×10^2 THz, while maps (b) and (d) illustrate the quartered PhC at a frequency of 2.9×10^2 THz

illustrate the behavior of guided and diffracted waves through the superlattice assembly, while Fig. 11(c) and Fig. 11(d) show the corresponding out-of-plane electric fields at two distinct frequencies: 0.7×10^2 THz and 3×10^2 THz.

The out-of-plane electric field E_z is properly steered below the Bragg limit, while the plane wave is disrupted above this critical frequency, which captures the inadequacy of typical PhCs in conducting high-frequency photons. High-frequency guided waves are demonstrated employing our new suggested technique that avoids the diffraction limit. Figure 12(a) and Fig. 12(b)

Optics EXPRESS

demonstrate the capacity of the anisotropic effect to effectively guide optical waves in halved and quartered cermet-type PhCs at much higher frequencies, specifically at 1.4×10^2 THz and 2.9×10^2 THz, respectively. This allows for overcoming the previously unavoidable diffraction constraint. The behavior of the out-of-plane electric field E_z within the defect is provided for both cases in Fig. 12(c) and Fig. 12(d), indicating that the guided waves remain unaltered due to the introduction of the anisotropic geometry effect.

5. Conclusion

This work reports on the use of an anisotropic architectural approach as a reliable way to circumvent the diffraction limit in two regular dielectric PhC configurations. This method has numerous far-reaching consequences and provides a new avenue for manipulating electromagnetic waves at high frequencies. It is also worth emphasizing that these findings can be expended and applied to other disciplines, including phononics or elastodynamics, to attain tiny devices operating at much higher frequencies, thereby pushing beyond the levels of miniaturization currently available. Besides, both symmetric and asymmetric quartered dimer network-type photonic crystals were explored. The symmetric case remained diffraction-omitted, while the asymmetric case displayed a quasi-bound state in the continuum, resulting in a sharp peak in the transmission spectrum with a highly QF of up to 9.15×10^5. This latter feature is congruent with optical sensing requirements, making it a promising candidate for accurate sensing applications.

Funding. UTT Project Stratégique NanoSPR (OPE-2022-0293); the Graduate School (Ecole Universitaire de Recherche) "NANOPHOT" (ANR-18-EURE-0013);

Acknowledgments. We thank all of the authors for their invaluable contributions to this study, as without their participation, this project would not have come to fruition. Their unwavering commitment to dedicating their time, providing valuable insights and willingly sharing their experiences have made this endeavor possible. Thus, we extend our heartfelt thanks to all authors involved.

Disclosures. The authors declare no conflict of interest.

Data availability. Data underlying the results presented in this paper are not publicly available at this time but may be obtained from the authors upon reasonable request

References

1. C. M. Watts, X. Liu, and W. J. Padilla, "Metamaterial electromagnetic wave absorbers," Adv. Mater. **24**(23), OP98–OP120 (2012).
2. V. M. Shalaev, W. Cai, U. K. Chettiar, H.-K. Yuan, A. K. Sarychev, V. P. Drachev, and A. V. Kildishev, "Negative index of refraction in optical metamaterials," Opt. Lett. **30**(24), 3356–3358 (2005).
3. J. Valentine, S. Zhang, T. Zentgraf, E. Ulin-Avila, D. A. Genov, G. Bartal, and X. Zhang, "Three-dimensional optical metamaterial with a negative refractive index," Nature **455**(7211), 376–379 (2008).
4. S. John, "Strong localization of photons in certain disordered dielectric superlattices," Phys. Rev. Lett. **58**(23), 2486–2489 (1987).
5. M. Sigalas and E. Economou, "Band structure of elastic waves in two dimensional systems," Solid State Commun. **86**(3), 141–143 (1993).
6. E. Yablonovitch, "Inhibited spontaneous emission in solid-state physics and electronics," Phys. Rev. Lett. **58**(20), 2059–2062 (1987).
7. T. F. Krauss, R. M. D. L. Rue, and S. Brand, "Two-dimensional photonic-bandgap structures operating at near-infrared wavelengths," Nature **383**(6602), 699–702 (1996).
8. L. Rayleigh, "Xvii. on the maintenance of vibrations by forces of double frequency, and on the propagation of waves through a medium endowed with a periodic structure," Lond. Edinb. Dublin philos. mag. j. sci. **24**(147), 145–159 (1887).
9. M. Lončar, T. Doll, J. Vučković, and A. Scherer, "Design and fabrication of silicon photonic crystal optical waveguides," J. Lightwave Technol. **18**(10), 1402–1411 (2000).
10. M. Estevez, M. Alvarez, and L. Lechuga, "Integrated optical devices for lab-on-a-chip biosensing applications," Laser & Photon. Rev. **6**(4), 463–487 (2012).
11. H. Kurt and D. S. Citrin, "Graded index photonic crystals," Opt. Express **15**(3), 1240–1253 (2007).
12. E. Ozbay, "Plasmonics: Merging photonics and electronics at nanoscale dimensions," Science **311**(5758), 189–193 (2006).
13. L. N. Quan, J. Kang, C.-Z. Ning, and P. Yang, "Nanowires for photonics," Chem. Rev. **119**(15), 9153–9169 (2019). PMID: 31282661.

Optics EXPRESS

14. I. V. Doronin, E. S. Andrianov, and A. A. Zyablovsky, "Overcoming the diffraction limit on the size of dielectric resonators using an amplifying medium," Phys. Rev. Lett. **129**(13), 133901 (2022).
15. M. Born and E. Wolf, *Principles of optics: electromagnetic theory of propagation, interference and diffraction of light* (Elsevier, 2013).
16. T. W. Ebbesen, H. J. Lezec, H. Ghaemi, T. Thio, and P. A. Wolff, "Extraordinary optical transmission through sub-wavelength hole arrays," Nature **391**(6668), 667–669 (1998).
17. D. K. Gramotnev and S. I. Bozhevolnyi, "Plasmonics beyond the diffraction limit," Nat. Photonics **4**(2), 83–91 (2010).
18. D. Lu and Z. Liu, "Hyperlenses and metalenses for far-field super-resolution imaging," Nat. Commun. **3**(1), 1205 (2012).
19. W. L. Barnes, A. Dereux, and T. W. Ebbesen, "Surface plasmon subwavelength optics," Nature **424**(6950), 824–830 (2003).
20. A. I. Kuznetsov, A. E. Miroshnichenko, M. L. Brongersma, Y. S. Kivshar, and B. Luk'yanchuk, "Optically resonant dielectric nanostructures," Science **354**(6314), aag2472 (2016).
21. J. B. Pendry, "Negative refraction makes a perfect lens," Phys. Rev. Lett. **85**(18), 3966–3969 (2000).
22. D. Schurig, J. J. Mock, B. J. Justice, S. A. Cummer, J. B. Pendry, A. F. Starr, and D. R. Smith, "Metamaterial electromagnetic cloak at microwave frequencies," Science **314**(5801), 977–980 (2006).
23. N. I. Landy, S. Sajuyigbe, J. J. Mock, D. R. Smith, and W. J. Padilla, "Perfect metamaterial absorber," Phys. Rev. Lett. **100**(20), 207402 (2008).
24. M. Khorasaninejad, W. T. Chen, R. C. Devlin, J. Oh, A. Y. Zhu, and F. Capasso, "Metalenses at visible wavelengths: Diffraction-limited focusing and subwavelength resolution imaging," Science **352**(6290), 1190–1194 (2016).
25. V. G. Veselago, "Properties of materials having simultaneously negative values of the dielectric and magnetic susceptibilities," Soviet Physics Solid State USSR **8**, 2854–2856 (1967).
26. M. Wegener, "Metamaterials beyond optics," Science **342**(6161), 939–940 (2013).
27. E. N. Economou and M. M. Sigalas, "Classical wave propagation in periodic structures: Cermet versus network topology," Phys. Rev. B **48**(18), 13434–13438 (1993).
28. J. D. Joannopoulos, R. Meade, and J. N. Winn, "Photonic crystals," Molding the flow of light (1995).
29. J. Joannopoulos, P. R. Villeneuve, and S. Fan, "Photonic crystals," Solid State Commun. **102**(2-3), 165–173 (1997). Highlights in Condensed Matter Physics and Materials Science.
30. P. S. J. Russell, "Optics of floquet-bloch waves in dielectric gratings," Appl. Phys. B **39**(4), 231–246 (1986).
31. F. Priolo, T. Gregorkiewicz, M. Galli, and T. F. Krauss, "Silicon nanostructures for photonics and photovoltaics," Nat. Nanotechnol. **9**(1), 19–32 (2014).
32. M. Hochberg and T. Baehr-Jones, "Towards fabless silicon photonics," Nat. Photonics **4**(8), 492–494 (2010).
33. Z. Chen, A. Taflove, and V. Backman, "Photonic nanojet enhancement of backscattering of light by nanoparticles: a potential novel visible-light ultramicroscopy technique," Opt. Express **12**(7), 1214–1220 (2004).
34. S. Han, P. Pitchappa, W. Wang, Y. K. Srivastava, M. V. Rybin, and R. Singh, "Extended bound states in the continuum with symmetry-broken terahertz dielectric metasurfaces," Adv. Opt. Mater. **9**(7), 2002001 (2021).
35. S. Joseph, S. Pandey, S. Sarkar, and J. Joseph, "Bound states in the continuum in resonant nanostructures: an overview of engineered materials for tailored applications," Nanophotonics **10**(17), 4175–4207 (2021).
36. S. Kolodny and I. Iorsh, "Q/v enhancement of micropillar resonator in bound states in the continuum regime," Opt. Lett. **45**(1), 181–183 (2020).
37. L. Vertchenko, C. DeVault, R. Malureanu, E. Mazur, and A. Lavrinenko, "Near-zero index photonic crystals with directive bound states in the continuum," Laser & Photonics Reviews **15**(7), 2000559 (2021).
38. C. Zhou, L. Huang, R. Jin, L. Xu, G. Li, M. Rahmani, X. Chen, W. Lu, and A. E. Miroshnichenko, "Bound states in the continuum in asymmetric dielectric metasurfaces," Laser & Photonics Reviews **17**(3), 2200564 (2023).
39. W. Lamb, D. M. Wood, and N. W. Ashcroft, "Long-wavelength electromagnetic propagation in heterogeneous media," Phys. Rev. B **21**(6), 2248–2266 (1980).
40. S. Fan, S. G. Johnson, J. D. Joannopoulos, C. Manolatou, and H. A. Haus, "Waveguide branches in photonic crystals," J. Opt. Soc. Am. B **18**(2), 162–165 (2001).
41. C. M. Soukoulis, *Photonic band gaps and localization*, Vol. 308 (Springer Science & Business Media, 2014), p. 91660M.